Electrochemical synthesis of ammonia based on Co_3Mo_3N catalyst and $LiAlO_2$-$(Li,Na,K)_2CO_3$ composite electrolyte

Ibrahim A. Amar, Rong Lan, Christophe T.G. Petit and Shanwen Tao*

Department of Chemical & Process Engineering, University of Strathclyde, Glasgow G1 1XJ, UK

Abstract

Cobalt molybdenum nitride (Co_3Mo_3N) catalyst was synthesised through ammonolysis of the corresponding precursors by flowing pure ammonia gas. The catalyst was characterised by x-ray diffraction (XRD) and scanning electron microscopy (SEM). Ammonia was successfully synthesised from wet hydrogen and dry nitrogen at atmospheric pressure using Co_3Mo_3N-Ag composite as cathode, Ag-Pd alloy as anode and $LiAlO_2$-$(Li/Na/K)_2CO_3$ composite as an electrolyte. Ammonia formation was investigated at 400, 425 and 450 ºC and the maximum observed ammonia formation rate was 3.27×10^{-10} mol s^{-1} cm^{-2} at 450 ºC when applied 0.8 V. The catalytic activity of Co_3Mo_3N for electrochemical ammonia synthesis is lower than that of Pd. The successful synthesis of ammonia demonstrates that $LiAlO_2$-$(Li/Na/K)_2CO_3$ composite exhibits protonic or/and oxygen ion conduction.

Keywords: electrochemical synthesis of ammonia; nitrides; Co_3Mo_3N; oxide-carbonate composite electrolyte

---

* Corresponding author:

Department of Chemical and Process Engineering,

University of Strathclyde, Glasgow G1 1XJ, UK

Tel. +44 (0) 141 548 2361; Fax: +44 (0) 141 548 2539
E-mail: shanwen.tao@strath.ac.uk

1. Introduction

Ammonia (NH_3) is the second most produced chemical in the world. It is an important intermediate in the manufacture of urea, nitric acid, ammonium nitrate, ammonium sulphate and ammonium phosphate [1]. Currently, the Haber-Bosch process is the dominant route for producing ammonia at large-scale. By this process, over 150 million metric tons of ammonia is produced per annum of which ~ 80 % is consumed in fertiliser industry [1, 2]. However, Haber-Bosch process suffers from the following drawbacks: high working pressure, high energy consumption and low conversion (10-15 %) [1]. The ammonia industry consumes more than 1 % of energy generated in the world and releases a large amount of CO_2 due to the use of natural gas or coal in this process [3]. The electrochemical process is regarded as one of the most promising alternatives to the conventional ammonia synthesis process [4, 5]. To synthesise ammonia from renewable electricity can significantly reduce CO_2 emission and alleviate the pressure on renewable electricity storage as well [6]. It has been reported that ammonia was produced in liquid electrolyte through reduction of N_2 [7, 8]. Ammonia synthesis based on low temperature proton-conducting electrolyte has also been reported. In 1998, Marnellos and Stoukides [9] reported electrochemical synthesis of ammonia from H_2 and N_2 under atmospheric pressure and at 570 °C. In that study a proton conductor ($SrCe_{0.95}Yb_{0.05}O_{3-\delta}$, SCYb) was used as a solid electrolyte and a porous Pd was used as both cathode and anode. It was found that ~ 78 % of the protons (H^+) transported through the electrolyte to the cathode was converted into ammonia. Since then, ammonia has been synthesised electrochemically using different proton conducting-based electrolytes [3, 10-17].

Transition metal nitrides (TMNs) have been investigated for a wide range of applications due to their magnetic, optical, magnetic and catalytic properties [18-20]. These materials, such as chromium nitride (CrN) and molybdenum nitride (Mo_2N), have been proposed as potential electrocatalysts for application in proton exchange membrane fuel cells (PEMFCs) to replace noble-metal based catalysts, such as the Pt group, that involve high cost and limited supply [21, 22]. In addition, bimetallic Mo-containing nitrides (e.g. Co_3Mo_3N) exhibit excellent catalytic properties in conventional ammonia synthesis from H_2 and N_2 [23-26]. This is due to the high ability of molybdenum to dissociate the dinitrogen molecule (N_2) [20, 27]. It was found that 2mol% Cs added Co_3Mo_3N gave the maximum activity after the reactant gas treatment and this catalyst gave higher productivity of ammonia than a double promoted iron catalyst [24, 27]. Therefore Co_3Mo_3N is potentially a good catalyst for electrochemical synthesis of ammonia.

To the best of our knowledge, there is no report on the electrochemical synthesis of ammonia based on Co_3Mo_3N catalyst. In this paper, for the first time, the electrochemical synthesis of ammonia from H_2 and N_2 using Co_3Mo_3N catalyst in a solid state electrolytic cell.

2. Experimental

2.1 Materials synthesis

Co_3Mo_3N was synthesised by nitriding the corresponding precursors according to the procedure reported by Mckay et al [25]. The precursor was obtained by mixing an aqueous solution of cobalt nitrate ($Co(NO_3)_2 \cdot 6H_2O$, Sigma Aldrich, 98 + %) with an aqueous solution of ammonium heptamolybdate ($(NH_4)_6Mo_7O_{24} \cdot H_2O$, Alfa Aeser, 99 %) with molar ratio of Co:Mo as 1:1. The mixed solution was evaporated on a hot-plate under magnetic agitation and a purple solid product was obtained. The cobalt molybdenum nitride catalyst was synthesised via a temperature-programmed reduction (TPR) of the corresponding precursor by flowing pure ammonia gas (BOC) in a heated quartz tube. Approximately 2 g of the desired material was put in a ceramic boat and placed in the heating zone of a tube furnace which was programmed to heat in three steps as follows: the temperature was increased from room temperature to 357 ºC at a rate of 5.6 ºC min^{-1}, and then slowly from 357 to 447 ºC at 0.5 ºC min^{-1}, then to 785 ºC at 2.1 ºC min^{-1} and then held for 5 hours at this temperature [28]. The furnace was then cooled to room temperature at a rate of 5 ºC min^{-1} in flowing ammonia. Since the nitrided material is air sensitive, it was passivated for 1 h in flowing N_2 gas to avoid oxidation. Finally, an ultrafine black powder of Co_3Mo_3N was obtained.

2.2 Pellet preparation for conductivity measurement

Composite electrolyte consisting of $LiAlO_2$-$(Li/Na/K)_2CO_3$ (50:50 wt %) was prepared as described elsewhere [29]. The AC conductivity measurements were carried out using a computer-controlled Solartron Analytical 1470E with AC amplitude of 100 mV over the frequency range 1 MHz - 0.01 Hz and 10 points per decade. The $LiAlO_2$-$(Li/Na/K)_2CO_3$ composite powder was uniaxially dry-pressed under 295 MPa into pellets with diameter of 13 mm and thickness of 2 mm. The green pellets were then sintered in air at 600 ºC for 2 h, at a heating/cooling rate of 2 ºC/min. Ag paste was brushed on both sides of the sintered pellets and fired at 600 °C for 30 minutes before the conductivity measurements. AC impedance

measurements were performed in three atmospheres, air, dry O_2 (dried through 98% H_2SO_4) and wet (~ 3% H_2O) 5% H_2/Ar. The measurements were carried out in the temperature range of 300-600 ºC.

2.3 Materials Characterisation

X-ray diffraction (XRD) data were collected at room temperature using a Bruker-AXS (D8A dvance) machine controlled by DIFFRACT plus™ software in the Bragg-Brentano reflection geometry with CuKα radiation (λ=1.5405 Å), fitted with a LynxEye^{TM} detector. XRD patterns were recorded in the 2θ range 5-85º with a step size of 0.009º and step time of 61.6 s at each step during data collection.

2.4 Fabrication of the single cell for ammonia synthesis

The electrolyte supported cell was fabricated by uniaxial dry-pressing the composite electrolyte powder ($LiAlO_2$-carbonate at 50:50 wt %) into a pellet with diameter of 19 mm under 121 MPa. The green pellet was sintered in air at 600 °C. The composite cathode was prepared by mixing the as-prepared Co_3Mo_3N catalyst with Ag paste to increase its conductivity and adhesion to the electrolyte surface. Then the Co_3Mo_3N-Ag composite was pasted on one side of the composite electrolyte as the cathode, with a surface area of 0.98 cm^2. Ag-Pd (Johnson Matthey, 20 wt % Pd) paste was painted on the other side as the anode. Ag wires were used as output terminals for both electrodes.

2.5 Ammonia synthesis

The fabricated single cell was placed in a self-designed double-chamber reactor. The electrolytic cell for ammonia was constructed as follows: Ag-Pd|$LiAlO_2$-carbonate|Co_3Mo_3N-Ag. The cathode chamber was fed with oxygen-free N_2 (BOC Gas), whereas the anode chamber was fed with wet, highly pure H_2 (BOC, 99.995%). The voltage was applied by a Solartron 1287A electrochemical interface controlled by software CorrWare/CorrView for automatic data collection. Constant voltage was applied and the ammonia synthesised at the cathode chamber was absorbed by 25 ml of dilute sulphuric acid (0.001 M) for 2 h. The concentration of NH_4^+ in the absorbed solution was analysed using Nessler's reagent (Aldrich). The produced

ammonia was detected using an ammonia meter (Palintest 1000) and the rate of ammonia formation was calculated using **Error! Reference source not found.**:

$$r_{NH_3} = \frac{[NH_4^+] \times V}{t \times A} \quad (1)$$

where $[NH_4^+]$ is the measured NH_4^+ ion concentration, V is the volume of the diluted H_2SO_4 used for ammonia collection, t is the absorption time and A is the effective area of the catalyst [13, 29]. The average Faraday efficiency was calculated through the total charge in column recorded by the Solartron 1287A during the measurements and real collected ammonia during that period of time [16].

AC impedance spectroscopy (IS) measurements were performed using a Schlumberger Solarton SI 1250 analyser, coupled with a SI 1287 Electrochemical Interface controlled by Z-plot/Z-view software. The AC impedance spectra were recorded over the frequency range 65 kHz to 0.01 Hz.

3. Results and discussion

3.1 XRD analysis

Fig. 1 shows the XRD pattern for the Co_3Mo_3N catalyst. A single phase of Co_3Mo_3N was obtained and was indexed as the cubic cell of Co_3Mo_3N (ICSD code 162273). The small weak peak at ~ 36 ° belongs to the strongest peak of Mo_2N (PDF No. 01-075-1150). The small peak at ~ 68 ° does not belong to known pure element or compounds composed of element Co, Mo, N and O. The crystallite sizes of the nitride catalyst was the range of 29 nm, estimated from Sherrer's formula [30].

$$D = \frac{k\lambda}{\beta \cos\theta} \quad (2)$$

where D is average particle size, k is a dimensionless shape factor (we used k = 0.9); λ is the X-ray wavelength; β is the line broadening at half the maximum intensity (FWHM), after

subtracting the instrumental line broadening, in radians; θ is the Bragg angle. The XRD pattern of $LiAlO_2$-$(Li,Na,K)_2CO_3$ composite has been reported in a previous study [29].

3.2 The ionic conductivity of the composite electrolyte

The ionic conductivities of the composite electrolyte in three different atmospheres (air, dry O_2 and wet 5% H_2-Ar) as function of temperature are shown in Fig. 2. It is to be noted that since the bulk and grain boundary contributions cannot be separated, only the total conductivity was plotted. As can be seen, the ionic conductivities of the composite electrolyte increase with increasing the operating temperature in all atmospheres. In addition, it can be clearly noticed that the conductivities changed at two different regions: below and above ~ 400 ºC, which is the melting point of the ternary carbonate ($(Li/Na/K)_2CO_3$) [31]. This conductivity jump phenomenon above the carbonate melting point has also been observed for doped ceria-ternary carbonate composite (SDC-$(Li/Na/K)_2CO_3$) [32], doped ceria-binary carbonate composite (e.g. SDC- or GDC-$(Li/Na)_2CO_3$) [33, 34] and non-ceria-binary carbonate composite (e.g. $LiAlO_2$- or LSGM-$(Li/Na)_2CO_3$) [35, 36].

Within the temperature range 600-400 ºC, the total conductivities were 0.215-0.048 S cm^{-1}, 0.218-0.037 S cm^{-1} and 0.217-0.047 S cm^{-1} in air, dry O_2 and wet 5% H_2-Ar respectively. It is well known that $LiAlO_2$ is an insulator [35]; therefore the ionic conduction in $LiAlO_2$-carobonate composite is likely to be due the carbonate plus the composite effect. The apparent activation energies (E_a) of the composite electrolyte at high temperature (600-400 ºC) under different atmospheres were extracted from the slope of each series of points in the Arrhenius plots of conductivity, as shown in the inset of Fig. 2. The activation energies were found to be 0.35(5) eV, 0.37(9) eV and 0.45(7) eV for the composite electrolyte in air, dry O_2 and wet 5% H_2-Ar respectively.

As mentioned above, enhancement in the ionic conductivities has been observed above the melting point of the ternary carbonate. At high temperature, the ternary carbonate in the composite will melt, which greatly enhances the mobility of both anions and cations, leading to superionic conduction. This means that all mobile ions (i.e. Li^+, Na^+, K^+, O^{2-}, H^+, HCO_3^- and CO_3^{2-}) contribute to the overall measured ionic conductivity [35]. However, it has been demonstrated that, during the electrolysis, only H^+ or O^{2-} are transported through the doped ceria-carbonate composite electrolyte, depending on the mode of operation (i.e. H^+ or O^{2-}

conduction in the electrolyte) and the other mobile ions (i.e. Li^+, Na^+, K^+, HCO_3^- and CO_3^{2-}) are blocked at the electrodes [37]. Similar behaviour is expected in the case of electrochemical synthesis of ammonia in an electrolytic cell based on $LiAlO_2$-carbonate composite electrolyte, in which only protons will be transported through the electrolyte, whereas other mobile ions will be blocked.

At low temperature (375-300 ºC), the ionic conductivities of the composite electrolyte dropped significantly and were found to be 0.005-4.653 × 10^{-5}, 0.018-1.235 × 10^{-5} and 0.027-3.719 × 10^{-4} S cm^{-1} in air, dry O_2 and wet 5% H_2-Ar respectively. This could be due to the fact that the conducting ions are less mobile below the melting point of the carbonates, leading to low ionic conductivities in this region. It should be noted that, below the carbonate melting point, the conductivities of the composite electrolyte in wet 5 % H_2-Ar were higher than those obtained in air and dry O_2. This could be due to the fact that that proton conduction can be easily activated at low temperature, compared to oxygen-ion conduction [37, 38]. In addition, the steam in wet 5%H_2/Ar might diffuse into the interfaces in $LiAlO_2$-$(Li/Na/K)_2CO_3$ composite, facilitate the transfer of protons, resulting in enhanced proton conductivity. At a temperature above 400 °C, the conductivity of the composite is dominant by the CO_3^{2-} ionic conduction thus the effect of proton conduction is not significant. Thus the conductivity of the composite are at similar level at different atmospheres when the temperature is above 400 °C.

It has been reported that the conductivity enhancement of the composites or two phase system occurs via the interface at which the ionic transport is fast [39]. Unlike doped ceria-carbonate composite electrolytes (e.g. SDC-carbonate), in which O^{2-} could be conducted through both the SDC phase and the interface between the two phases. $LiAlO_2$ is not an oxygen ion conductor and the O^{2-} conduction in the $LiAlO_2$-$(Li/Na/K)_2CO_3$) composite is likely to occur only through the interface between the two phases (i.e. $LiAlO_2$ and carbonate). This indicates that the O^{2-} conduction mechanism in $LiAlO_2$-carbonate composite is different from that in the doped ceria-carbonate composite electrolytes [35]. On the other hand, the H^+ conduction in the $LiAlO_2$-$(Li/Na/K)_2CO_3$) composite is similar to that of doped ceria-carbonate composites, which is believed to occur through the interface between the two phases (i.e. the oxide and carbonate). In an H_2 containing atmosphere, some bicarbonates (HCO_3^-) may be formed through the reaction between the carbonates (CO_3^{2-}) and H_2. Thus, protons may be transported between CO_3^{2-} ions in the form of HCO_3^-, which may lead to proton conduction [35, 38, 40].

3.3 Synthesis of ammonia at different temperatures

Fig. 3 shows the electrolytic cell performance stabilities during the synthesis of ammonia at different temperatures (400-450 °C) with an applied voltage of 0.8 V for an electrolytic cells based on Co_3Mo_3N-Ag composite cathode. It was noticed that the cell demonstrated almost stable performance at all investigated temperatures. At low operating temperature (400 °C), the generated current density decreased significantly during the first 60 min, after which an almost stable current was generated. This could be attributed to the blocking effects which has been observed in the oxide-carbonate composite materials [17, 41]. Under applied dc voltage, the cations such as Li^+, Na^+ and K^+ ions may transfer to the cathode side, forming a positive charged layer on the electrolyte side on the electrolyte/cathode interface. This positively charged layer may partially block the transfer of H^+ ions leading to reduced current density. At a higher operating temperatures (425 and 450 °C), the electrolytic cell exhibited a stable performance and generated almost the same current density (~ 3.2 mA/cm^2).

Fig. 4a shows the AC impedance spectra under open circuit conditions for the electrolytic cell based on Co_3Mo_3N-Ag composite cathode, at different temperatures (400-450 °C). It should be noted that two depressed semicircles were observed, suggesting that there are at least two electrode processes. The impedance data were fitted using Zview software with an equivalent circuit model of the type LRs(R1CPE1)(R2CPE2), as shown in Fig. 4b. Here, L represents the inductance caused by the equipment and wire connections, Rs is the series resistance, which comprises the resistances of the electrolyte, electrode materials and the contact resistance at the electrode/electrolyte interfaces; the two components (R1CPE1) and (R2CPE2) in series are associated with the electrode processes at high and low frequency arcs respectively. R1 and R2 represent the polarisation resistance while CPE is a constant phase element which represents a non-ideal capacitor (C). The characteristic capacitances for the high frequency semicircles (HF) were found to be in the range of 10^{-5}-10^{-4} F/cm^2, which could be attributed to the charge transfer processes at the electrode/electrolyte interface. The low frequency semicircle (LF) with the associated capacitances of 10^{-4}-10^{-2} F/cm^2 could be ascribed to the mass transfer processes at the electrode [42-45]. In addition, the Rs resistance, which mainly related to the ohmic resistance of the electrolyte, decreased significantly when increasing the cell operating temperature from 400 to 450 °C. This could be attributed to the enhancement in the ionic conductivity of the composite electrolyte at increased operating temperature. With increasing

the operating temperature of the electrolytic cell, there was also a significant decrease in the total polarisation resistance (Rp), which is the sum of R1 and R2. This could be due to the improvement in the electrochemical process of both cathode and anode at elevated temperatures.

Fig. 5 shows the effect of cell operating temperature on the ammonia formation rate in electrolytic cell based on Co_3Mo_3N-Ag composite cathodes. This effect was investigated by varying the operating temperature (400-450 °C) and keeping the cell voltage at constant value of 0.8 V over a period of 2 h. The ammonia produced in the cathode chamber was absorbed by 25 ml of diluted sulphuric acid. When Nessler's reagent was added to the absorbed solution. The colour immediately changed to yellow when Nessler's reagent was added into the H_2SO_4 solution after ammonia collection. This indicates that NH_4^+ is present in the absorbed solution and thus that ammonia was successfully synthesised. As can be seen from Fig. 5, the ammonia formation rate decreased slightly when the operating temperature was raised from 400 ºC to 425 ºC. Moreover, a significant increase in the rate of ammonia formation was obtained by further increasing the temperature to 450 ºC. The maximum rate was found to be 3.27×10^{-10} mol s^{-1} cm^{-2} at 450 ºC, at which the generated current density and the corresponding Faradaic efficiency were 3.21 mA/cm^2 and 2.95 % respectively. This increase in the ammonia formation rate at increased cell operating temperature could be attributed to the increased catalytic activity of Co_3Mo_3N. The other possibility is that the catalytic activity of nitride catalyst increases at higher temperatures. The obtained NH_3 formation rate is in general one order of magnitude lower than the one reported by Li et al. [46] (3.09×10^{-9} mol s^{-1} cm^{-2}) when Ag-Pd alloy was used as cathode catalyst, indicating the catalytic activity of Co_3Mo_3N is relatively lower than that for Pd. Ag was also used as conducting component in the Ru/MgO cathode for electrochemical synthesis of ammonia from N_2 and H_2O[47]. The low observed ammonia formation rate indicates that the catalytic activity of Ag on ammonia synthesis is very low. It can be also seen from Fig. 5 that, the Faradaic efficiency decreased from 1.57 % (2.53 mA/cm^2) to 0.95 % (3.24 mA/cm^2) with an increase in the operating temperature from 400 to 425 °C. With further increase in operating temperature (450 °C), the Faradaic efficiency increased and reached a value of 2.95 % at current density of 3.21 mA/cm^2. These low Faradaic efficiencies indicate that not all protons transported through the electrolyte to the cathode surface reacted with the adsorbed N_2 to form ammonia. This means that competitive hydrogen evolution reaction (HER) is the predominant process over the cathode surface [13, 48, 49]. It has been reported that the decomposition of Co_3Mo_3N may lead to the formation of impurities Mo_2N

and Co [27]. The existence of Mo_2N and unknown impurity in our catalyst may also lead to reduced catalytic activity thus lower ammonia formation rates when used as electrocatalyst.

3.4 Synthesis of ammonia at different applied voltages

Fig. 6 shows the performance of the electrolytic cell at 450 °C at different applied voltages (0.4-1.2 V). It can be seen that, the current is quite stable after a period of stabilising time. It could be explained that this increase in the current density with the voltage could be due to more protons being transported to the cathode [29]. However, decrease in current was observed when a voltage of 1.2V was applied indicating the ion blocking effects becomes more significant at higher applied voltage [17, 41]. At higher applied voltage, the positively charged layer due at the electrolyte/cathode interface due to the accumulation of Li^+, Na^+ and K^+ ions will be thicker which may partially block the transfer of protons, leading to reduced current density.

The effect of the applied voltages on the ammonia formation rate was investigated by keeping the cell operating temperature at 450 °C and varying the applied voltage from 0.4 to 1.2 V. As shown in Fig. 7, the ammonia formation rate increased significantly with the increase in the applied voltage. The maximum rate was obtained when the electrolytic cell operated at 0.8 V (3.27×10^{-10} mol s^{-1} cm^{-2}). However, at a voltage above 0.8 V, the rate decreased markedly and reached the minimum value when 1.2 V was applied. This decrease in the rate of ammonia formation at higher applied voltage might be due to the competitive adsorption between the N_2 and H_2 over the cathode surface [48, 49]. At high applied voltage, the current was also higher leading to high hydrogen evolution speed at the cathode. This will prevent the diffusion of N_2 onto the cathode surface to react with protons, forming ammonia. It can be also seen from Fig. 7, the Faradaic efficiencies decreased significantly with an increase in applied voltage. The maximum Faradaic efficiency of 3.83 % was attained when 0.4 V was imposed through the electrolytic cell. These low current efficiencies indicate that the hydrogen evolution reaction (HER) is the dominant process over the cathode surface [48, 49].

4. Conclusion

Cobalt molybdenum nitride (Co_3Mo_3N) was synthesised by ammonolysis and characterised by XRD and SEM. The ionic conductivity of the composite electrolyte was investigated under three different atmospheres (air, O_2 and 5% H_2-Ar). The ionic conductivity of the composite electrolyte ($LiAlO_2$-carbonate) was in the range of 0.22-10^{-5} S/cm with the measured temperature of 600-300 °C. The electrochemical synthesis of ammonia was investigated in electrolyte supported cell using, $LiAlO_2$-carbonate composite as an electrolyte, Co_3Mo_3N-Ag composite as a cathode and Ag-Pd alloy as an anode. The maximum rate of ammonia formation was found to be 3.27×10^{-10} mol s^{-1} cm^{-2} at 450 ºC and 0.8 V. The catalytic activity of Co_3Mo_3N for electrochemical ammonia synthesis is lower than that of Pd. The successful synthesis of ammonia demonstrates that $LiAlO_2$-$(Li,Na,K)_2CO_3$ composite exhibits protonic or/and oxygen ion conduction.

Acknowledgement

The authors gratefully thank EPSRC SuperGen XIV 'Delivery of Sustainable Hydrogen' project (Grant No EP/G01244X/1) for funding. One of the authors (Ibrahim A. Amar) thanks The Libyan Cultural Affairs, London for support of his study in UK.

References

1. M. Appl, *Ammonia: principles and industrial practice*, Wiley-VCH Weinheim, Germany, 1999.
2. US and G. Survey, *Mineral Commodity Summaries*, Geological Survey, 2012.
3. R. Lan and S. W. Tao, RSC Adv., **3**, 18016-18021 (2013)
4. I. A. Amar, R. Lan, C. T. Petit and S. W. Tao, J. Solid State Electrochem., **15**, 1845-1860 (2011)
5. S. Giddey, S. P. S. Badwal and A. Kulkarni, Inter. J. Hydrogen Energy, **38**, 14576-14594 (2013)
6. R. Lan, J. T. S. Irvine and S. W. Tao, Inter. J. Hydrogen Energy, **37**, 1482-1494 (2012)
7. F. Koleli and D. B. Kayan, J. Electroanal. Chem., **638**, 119-122 (2010)
8. A. Tsuneto, A. Kudo and T. Sakata, J. Electroanal. Chem., **367**, 183-188 (1994)
9. G. Marnellos and M. Stoukides, Science, **282**, 98-100 (1998)
10. Z. J. Li, R. Q. Liu, Y. H. Xie, S. Feng and J. D. Wang, Solid State Ionics, **176**, 1063-1066 (2005)
11. Y. Guo, B. Liu, Q. Yang, C. Chen, W. Wang and G. Ma, Electrochem. Comm., **11**, 153-156 (2009)
12. W. Wang, X. Cao, W. Gao, F. Zhang, H. Wang and G. Ma, J. Memb. Sci., **360**, 397-403 (2010)
13. R. Lan, J. T. Irvine and S. W. Tao, Sci. Rep., **3**, 1145 (2013)
14. I. A. Amar, C. T. G. Petit, L. Zhang, R. Lan, P. J. Skabara and S. W. Tao, Solid State Ionics, **201**, 94-100 (2011)
15. I. A. Amar, C. T. G. Petit, G. Mann, R. Lan, P. J. Skabara and S. W. Tao, Inter. J. Hydrogen Energy, **39**, 4322-4330 (2014)
16. R. Lan, K. A. Alkhazmi, I. A. Amar and S. W. Tao, Electrochim. Acta, **123**, 582-587 (2014)
17. R. Lan, K. A. Alkhazmi, I. A. Amar and S. W. Tao, Appl. Catal. B: Environ., **152–153**, 212-217 (2014)
18. L. Roux, J. Hanus, J. Francois and M. Sigrist, Solar Energy Mater., **7**, 299-312 (1982)
19. W. R. Lambrecht, M. Miao and P. Lukashev, J. Appl. Phys., **97**, 10D306-310D306-303 (2005)
20. K.-i. Aika and A. Ozaki, J. Catal., **14**, 311-321 (1969)
21. H. Zhong, X. Chen, H. Zhang, M. Wang and S. S. Mao, Appl. Phys. Lett., **91**, 163103-163103-163103 (2007)
22. H. Zhong, H. Zhang, G. Liu, Y. Liang, J. Hu and B. Yi, Electrochem. Comm., **8**, 707-712 (2006)
23. R. Kojima and K.-i. Aika, Appl. Catal. A: General, **219**, 141-147 (2001)
24. C. J. Jacobsen, Chem. Comm., 1057-1058 (2000)
25. D. McKay, J. S. J. Hargreaves, J. L. Rico, J. L. Rivera and X. L. Sun, J. Solid State Chem., **181**, 325-333 (2008)
26. R. Kojima and K. Aika, Appl. Catal. A - General, **218**, 121-128 (2001)
27. R. Kojima and K.-i. Aika, Appl. Catal. A: General, **215**, 149-160 (2001)
28. J. S. J. Hargreaves and D. McKay, J. Molecular Catal. A - Chem., **305**, 125-129 (2009)

29. I. A. Amar, R. Lan, C. T. G. Petit, V. Arrighi and S. W. Tao, Solid State Ionics, **182**, 133-138 (2011)
30. M. M. El-Desoky, M. S. Al-Assiri and A. A. Bahgat, J. Alloys & Compds, **590**, 572-578 (2014)
31. G. J. Janz and M. R. Lorenz, J. Chem. & Eng. Data, **6**, 321-323 (1961)
32. C. Xia, Y. Li, Y. Tian, Q. Liu, Y. Zhao, L. Jia and Y. Li, J. Power Sources, **188**, 156-162 (2009)
33. J. Huang, Z. Mao, Z. Liu and C. Wang, Electrochem. Comm., **9**, 2601-2605 (2007)
34. R. Chockalingam and S. Basu, Inter. J. Hydrogen Energy, **36**, 14977-14983 (2011)
35. S. Li, X. Wang and B. Zhu, Electrochem. Comm., **9**, 2863-2866 (2007)
36. F. Xie, C. Wang, Z. Mao and Z. Zhan, Inter. J. Hydrogen Energy, **38**, 11085-11089 (2013)
37. B. Zhu, I. Albinsson, C. Andersson, K. Borsand, M. Nilsson and B.-E. Mellander, Electrochem. Comm., **8**, 495-498 (2006)
38. X. Wang, Y. Ma, S. Li, A.-H. Kashyout, B. Zhu and M. Muhammed, J. Power Sources, **196**, 2754-2758 (2011)
39. B. Nettelblad, B. Zhu and B.-E. Mellander, Phys. Rev. B, **55**, 6232-6237 (1997)
40. L. Zhang, R. Lan, A. Kraft and S. W. Tao, Electrochem. Comm., **13**, 582-585 (2011)
41. L. Fan, G. Zhang, M. Chen, C. Wang, J. Di and B. Zhu, Inter. J. Electrochem. Sci., **7**, 8420-8435 (2012)
42. S. Klinsrisuk, PhD Adobe Acrobat Document, 18 MB, University of St. Andrews, 2010.
43. S. Li, Z. Lü, N. Ai, K. Chen and W. Su, J. Power Sources, **165**, 97-101 (2007)
44. C.-H. Li, S.-H. Hu, K.-W. Tay and Y.-P. Fu, Ceram. Inter., **38**, 1557-1562 (2012)
45. J. T. S. Irvine, D. C. Sinclair and A. R. West, Adv. Mater., **2**, 132-138 (1990)
46. Z. J. Li, R. Q. Liu, J. D. Wang, Y. H. Xie and F. Yue, J. Solid State Electrochem., **9**, 201-204 (2005)
47. A. Skodra and M. Stoukides, Solid State Ionics, **180**, 1332-1336 (2009)
48. A. Sclafani, V. Augugliaro and M. Schiavello, J. Electrochem. Soc., **130**, 734-736 (1983)
49. V. Kordali, G. Kyriacou and C. Lambrou, Chem. Comm., 1673-1674 (2000)

Captions

Fig. 1 Powder X-ray diffraction pattern of Co_3Mo_3N, after nitridation

Fig. 2 The AC conductivity plot against temperature of $LiAlO_2$-$(Li/Na/K)_2CO_3$ composite electrolyte in air, dry O_2 and wet 5% H_2-Ar

Fig. 3 Electrolytic cell performance stability at 400, 425 and 450 °C at 0.8 V: The electrolytic cell was; wet H_2, Ag-Pd|$LiALO_2$-carbonate|Co_3Mo_3N-Ag, dry N_2

Fig. 4(a) Impedance spectra under open circuit conditions for electrolytic cell based on Co_3Mo_3N-Ag composite cathode at 400-450 °C; (b) An equivalent circuit for the impedance data

Fig. 5 Dependence of the rate of ammonia formation on the operating temperature. The electrolytic cell was; wet H_2, Ag-Pd|$LiALO_2$-carbonate|Co_3Mo_3N-Ag, dry N_2

Fig. 6 Electrolytic cell performance stability at 450 °C and 0.4-1.2 V: The electrolytic cell was; wet H_2, Ag-Pd|$LiALO_2$-carbonate|Co_3Mo_3N-Ag, dry N_2

Fig. 7 Dependence of the rate of ammonia formation on the applied voltage: The electrolytic cell was; wet H_2, Ag-Pd|$LiALO_2$-carbonate|Fe_3Mo_3N-Ag, dry N_2

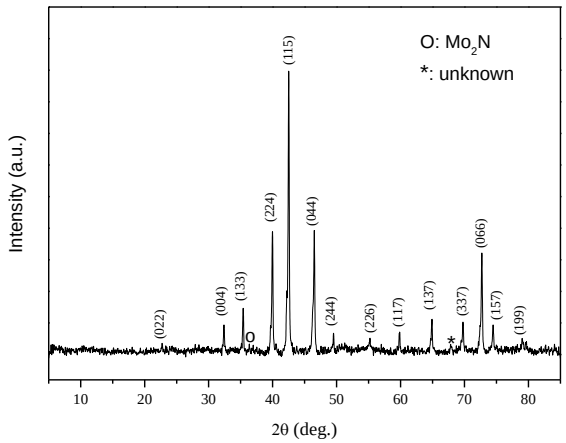

Fig. 1 Powder X-ray diffraction pattern of Co_3Mo_3N, after nitridation.

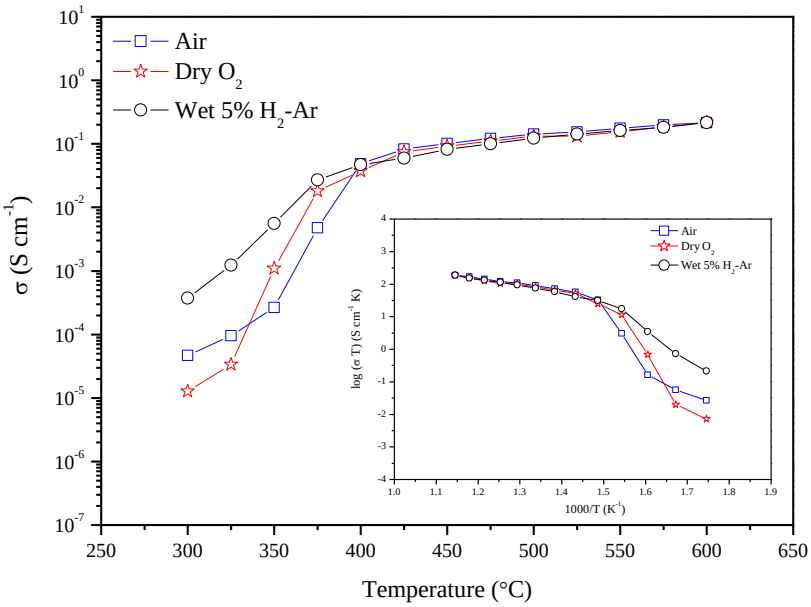

Fig. 2 The AC conductivity plot against temperature of $LiAlO_2$-$(Li/Na/K)_2CO_3$ composite electrolyte in air, dry O_2 and wet 5% H_2-Ar

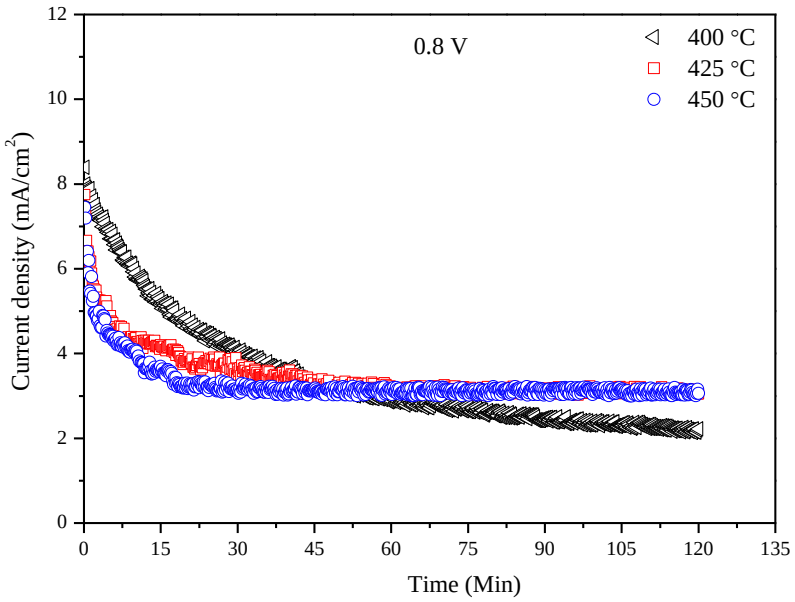

Fig. 3 Electrolytic cell performance stability at 400, 425 and 450 °C at 0.8 V: The electrolytic cell was; wet H_2, Ag-Pd|$LiALO_2$-carbonate|Co_3Mo_3N-Ag, dry N_2.

(a)

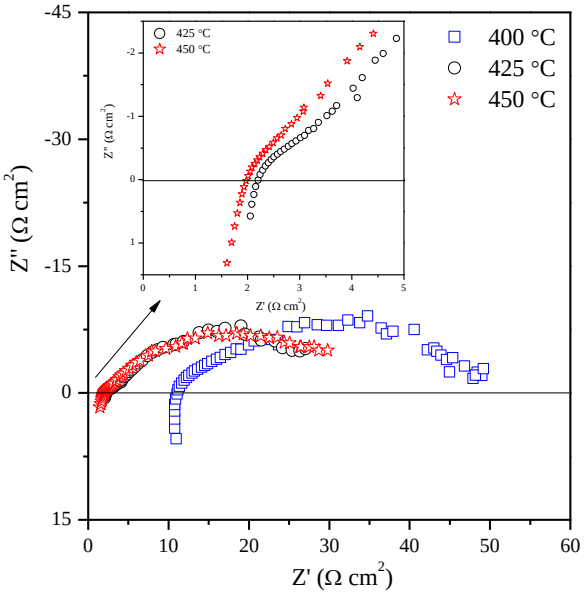

(b)

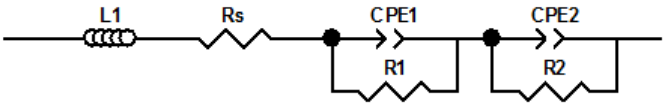

Fig. 4(a) Impedance spectra under open circuit conditions for electrolytic cell based on Co_3Mo_3N-Ag composite cathode at 400-450 °C; (b) An equivalent circuit for the impedance data

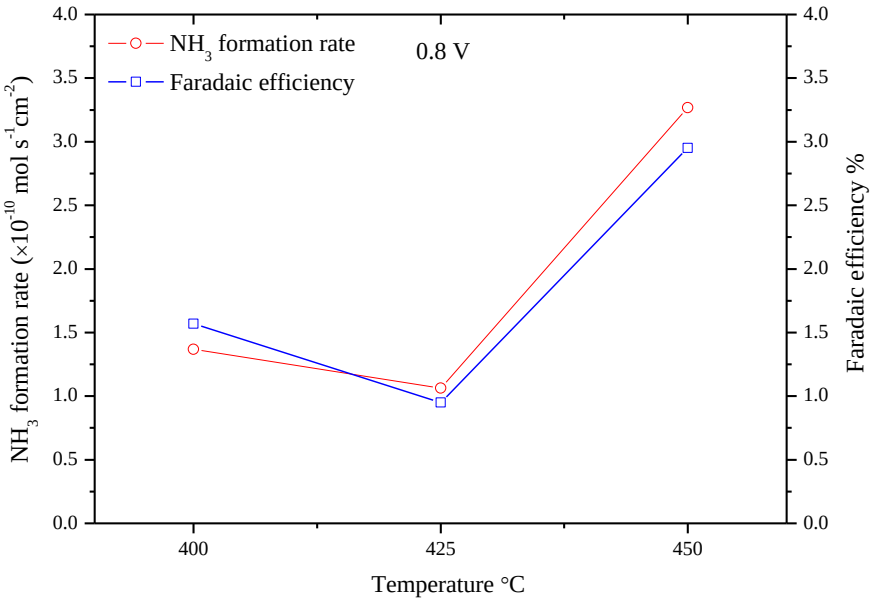

Fig. 5 Dependence of the rate of ammonia formation on the operating temperature. The electrolytic cell was; wet H_2, Ag-Pd|$LiALO_2$-carbonate|Co_3Mo_3N-Ag, dry N_2

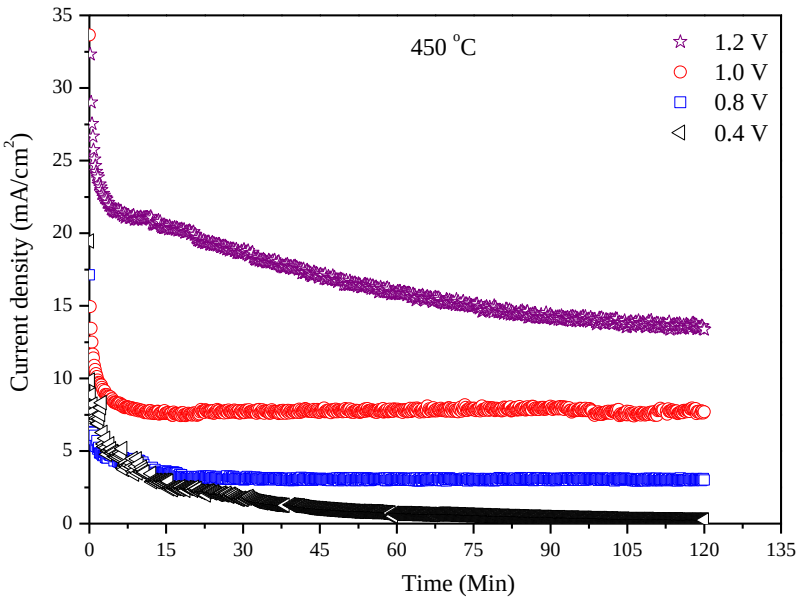

Fig. 6 Electrolytic cell performance stability at 450 °C and 0.4-1.2 V: The electrolytic cell was; wet H_2, Ag-Pd|$LiALO_2$-carbonate|Co_3Mo_3N-Ag, dry N_2

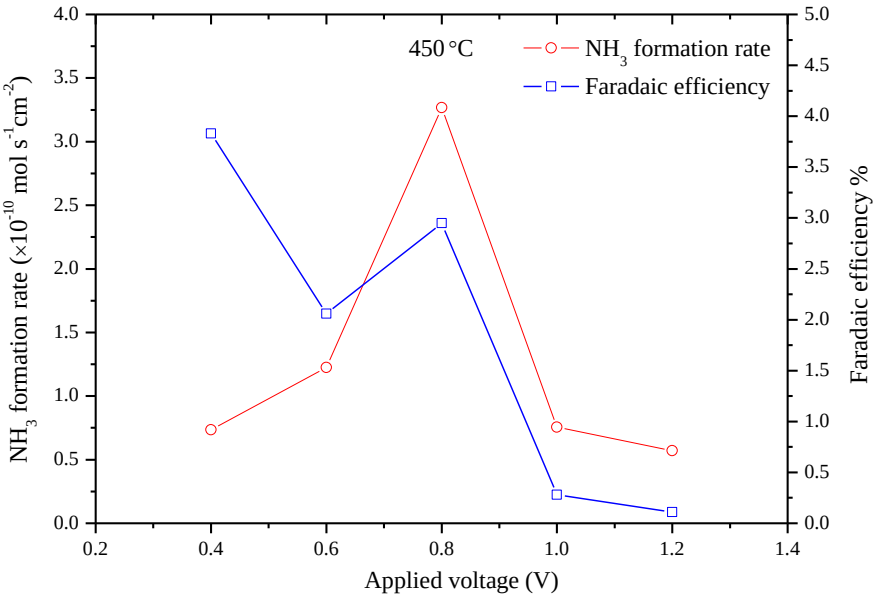

Fig. 7 Dependence of the rate of ammonia formation on the applied voltage: The electrolytic cell was; wet H_2, Ag-Pd|$LiALO_2$-carbonate|Fe_3Mo_3N-Ag, dry N_2.